Helical polynomial curves interpolating G^1 data with prescribed axes and pitch angles

Rida T. Farouki
Department of Mechanical and Aerospace Engineering,
University of California, Davis, CA 95616, USA.

Abstract

A helical curve, or curve of constant slope, offers a natural flight path for an aerial vehicle with a limited climb rate to achieve an increase in altitude between prescribed initial and final states. Every polynomial helical curve is a spatial Pythagorean–hodograph (PH) curve, and the distinctive features of the PH curves have attracted growing interest in their use for Unmanned Aerial Vehicle (UAV) path planning. This study describes an exact algorithm for constructing helical PH paths, corresponding to a constant climb rate at a given speed, between initial and final positions and motion directions. The algorithm bypasses the more sophisticated algebraic representations of spatial PH curves, and instead employs a simple "lifting" scheme to generate helical PH paths from planar PH curves constructed using the complex representation. In this context, a novel scheme to construct planar quintic PH curves that interpolate given end points and tangents, with exactly prescribed arc lengths, plays a key role. It is also shown that these helical paths admit simple closed–form rotation–minimizing adapted frames. The algorithm is simple, efficient, and robust, and can accommodate helical axes of arbitrary orientation through simple rotation transformations. Its implementation is illustrated by several computed examples.

Keywords: path planning, unmanned aerial vehicles, climb rate, arc length, Hermite interpolation, helical polynomial curves, Pythagorean–hodograph curves.

e–mail address: farouki@ucdavis.edu

1 Introduction

There has recently been considerable interest in using *Pythagorean–hodograph* (PH) *curves* to specify paths for swarms of unmanned aerial vehicles (UAVs) or other autonomous or remotely–operated vehicles [1, 3, 4, 6, 20, 21, 23, 24, 25, 26, 27, 28, 29, 30, 31, 33]. A polynomial PH curve $\mathbf{r}(\xi) = (x(\xi), y(\xi), z(\xi))$ incorporates a special algebraic structure [9], ensuring that the components of the hodograph (derivative) $\mathbf{r}'(\xi) = (x'(\xi), y'(\xi), z'(\xi))$ satisfy a Pythagorean condition — i.e., $x'^2(\xi)+y'^2(\xi)+z'^2(\xi)$ is equal to the perfect square of a single polynomial. This feature facilitates *exact* computations of various properties required to satisfy geometrical or physical path constraints — such as bounds on path curvature or climb angle, avoidance of obstacles, and maintenance of safe vehicle separations. An overview of the capabilities of PH curves within the context of UAV path planning may be found in [13].

The goal of the present study is to elucidate a simple and exact PH curve solution to a basic path planning problem — namely, to achieve an increase in altitude between states with prescribed initial/final positions and directions through a motion that corresponds to a fixed rate of climb at constant speed. UAV climb rates are inherently limited by considerations such as propulsive power, angle of attack, and stall avoidance, and rapid changes of altitude may be required to accommodate obstacle avoidance, meteorological conditions, remote sensing requirements, etc. The design of PH curve UAV paths under climb rate constraints has recently been studied by Neto and Campos [23, 24]. Although these studies employ the quaternion representation [5, 12] of spatial PH curves, a simpler approach to constructing climb–rate–limited paths is possible, based on the recognition that they must be *helical* curves.

A (generalized) helix is a space curve[1] $\mathbf{r}(\xi)$ whose tangent vector $\mathbf{t}(\xi) = \mathbf{r}'(\xi)/|\mathbf{r}'(\xi)|$ maintains a constant inclination ψ (the *pitch angle*) with a fixed unit vector $\mathbf{a}$ (the *axis* of the helix), i.e.,

$$\mathbf{a} \cdot \mathbf{t}(\xi) \equiv \cos\psi \,. \tag{1}$$

There are several alternative (equivalent) characterizations for helical curves [32] — including (1) a constant curvature to torsion ratio: $\kappa(\xi)/\tau(\xi) \equiv \tan\psi$; (2) the *tangent indicatix* (the curve traced on the unit sphere by the tangent vector $\mathbf{t}(\xi)$) is a small circle arc; and (3) the second, third, and fourth curve derivatives are linearly dependent: $[\,\mathbf{r}''(\xi) \times \mathbf{r}'''(\xi)\,] \cdot \mathbf{r}''''(\xi) \equiv 0$.

[1] It will be understood henceforth that we confine our attention to true space curves, since every planar curve is trivially helical.

In the present context, a key fact is that *every polynomial helical curve is a PH curve* [17]. This is evident upon writing (1) as $\mathbf{a} \cdot \mathbf{r}'(\xi) \equiv \cos\psi\, |\mathbf{r}'(\xi)|$. Since the left–hand side is a polynomial, the *parametric speed* $|\mathbf{r}'(\xi)|$ — i.e., the derivative $\mathrm{d}s/\mathrm{d}\xi$ of the arc length s with respect to the curve parameter ξ — must be a *polynomial* function of ξ. The characterization of polynomial helical curves has already been thoroughly investigated, and algorithms for their construction by the interpolation of discrete data have been formulated [2, 14, 15, 17, 22]. These algorithms utilize the sophisticated quaternion and Hop map forms [5] of spatial PH curves, and impose no *a priori* restriction on the orientation of the helical axis $\mathbf{a}$. In the UAV climb rate problem, however, the imposition of a vertical axis allows helical paths to be constructed using the simpler machinery of *planar* PH curves through a simple "lifting" process. The ability to construct planar PH curves satisfying specified end conditions with prescribed arc lengths [10] is a crucial element of this process.

The remainder of this paper is organized as follows. First, basic properties of the planar PH curves are summarized in Section 2, and an algorithm for the construction of planar PH quintics that precisely match specified end points, end tangents, and total arc length, is outlined in Section 3. Based upon this construction, Section 4 describes the "lifting" scheme that generates helical paths with vertical axes and specified pitch angles, between given end points and motion directions. Section 5 then derives the quaternion representation for these helical paths, and employs it to show how the solution scheme may be extended to accommodate helical axes of arbitrary orientation. It is also shown in Section 6 that the helical paths admit simple closed–form reductions for their rotation–minimizing frames. The methodology is summarized by an algorithm outline in Section 7, and its implementation is illustrated by some computed examples. Finally, Section 8 recapitulates the key results of this study, and suggests possible avenues for their generalization.

2 Planar Pythagorean–hodograph curves

The distinctive property of a plane polynomial PH curve $\mathbf{p}(\xi) = (x(\xi), y(\xi))$ is that the parametric speed $\sigma(\xi) = |\mathbf{p}'(\xi)|$ is simply a polynomial in ξ [19]. Consequently, PH curves possess rational unit tangents, normals, curvatures, and offset curves; their arc lengths are exactly computable; and they are well suited to real–time precision motion control applications [9].

A convenient approach to constructing and analyzing planar PH curves

is the complex representation [7], wherein a PH curve of degree $n = 2m + 1$ is generated from a degree–m complex "pre–image" polynomial

$$\mathbf{w}(\xi) \;=\; a(\xi) + \mathrm{i}\, b(\xi) \;=\; \sum_{k=0}^{m} \mathbf{w}_k \binom{m}{k} (1-\xi)^{m-k} \xi^k \tag{2}$$

with Bernstein coefficients $\mathbf{w}_k = a_k + \mathrm{i}\, b_k$, by integrating the relation

$$\mathbf{p}'(\xi) \;=\; x'(\xi) + \mathrm{i}\, y'(\xi) \;=\; \mathbf{w}^2(\xi) \;=\; a^2(\xi) - b^2(\xi) + \mathrm{i}\, 2\, a(\xi) b(\xi)\,. \tag{3}$$

The parametric speed, unit tangent, and curvature may be expressed [7] as

$$\sigma(\xi) \;=\; |\mathbf{w}(\xi)|^2\,, \quad \mathbf{t}(\xi) \;=\; \frac{\mathbf{w}^2(\xi)}{\sigma(\xi)}\,, \quad \kappa(\xi) \;=\; 2\,\frac{\mathrm{Im}(\overline{\mathbf{w}}(\xi)\mathbf{w}'(\xi))}{\sigma^2(\xi)}\,. \tag{4}$$

Since $\sigma(\xi)$ is a polynomial, its indefinite integral — the cumulative arc length function $s(\xi)$ — is likewise a polynomial, of degree n. The simplest planar PH curves suitable for free–form design are the quintics, generated by a quadratic $\mathbf{w}(\xi)$ with Bernstein coefficients $\mathbf{w}_0, \mathbf{w}_1, \mathbf{w}_2$. Integration of (3) yields [7] their Bézier control points $\mathbf{p}_k = x_k + \mathrm{i}\, y_k$ (with $\mathbf{p}_0$ an integration constant) as

$$\begin{aligned}
\mathbf{p}_1 \;&=\; \mathbf{p}_0 + \frac{1}{5}\,\mathbf{w}_0^2\,, \quad \mathbf{p}_2 \;=\; \mathbf{p}_1 + \frac{1}{5}\,\mathbf{w}_0\mathbf{w}_1\,, \\
\mathbf{p}_3 \;&=\; \mathbf{p}_2 + \frac{1}{5}\,\frac{2\mathbf{w}_1^2 + \mathbf{w}_0\mathbf{w}_2}{3}\,, \\
\mathbf{p}_4 \;&=\; \mathbf{p}_3 + \frac{1}{5}\,\mathbf{w}_1\mathbf{w}_2\,, \quad \mathbf{p}_5 \;=\; \mathbf{p}_4 + \frac{1}{5}\,\mathbf{w}_2^2\,.
\end{aligned} \tag{5}$$

The Bernstein coefficients of the parametric speed polynomial $\sigma(\xi)$ are

$$\begin{aligned}
\sigma_0 \;&=\; |\mathbf{w}_0|^2\,, \quad \sigma_1 \;=\; \mathrm{Re}(\overline{\mathbf{w}}_0\mathbf{w}_1)\,, \\
\sigma_2 \;&=\; \frac{2\,|\mathbf{w}_1|^2 + \mathrm{Re}(\overline{\mathbf{w}}_0\mathbf{w}_2)}{3}\,, \\
\sigma_3 \;&=\; \mathrm{Re}(\overline{\mathbf{w}}_1\mathbf{w}_2)\,, \quad \sigma_4 \;=\; |\mathbf{w}_2|^2\,.
\end{aligned} \tag{6}$$

Correspondingly, the arc length polynomial $s(\xi)$ has Bernstein coefficients

$$s_0 \;=\; 0 \qquad \text{and} \qquad s_k \;=\; \frac{1}{5}\sum_{j=0}^{k-1} \sigma_j\,, \quad k = 1, \ldots, 5 \tag{7}$$

and the total arc length is

$$S \;=\; s(1) \;=\; s_5 \;=\; \frac{\sigma_0 + \sigma_1 + \sigma_2 + \sigma_3 + \sigma_4}{5}\,. \tag{8}$$

3 G^1 planar PH quintics with prescribed arc lengths

It was demonstrated in [10] that planar quintic PH curves may be constructed with prescribed start/end points $\mathbf{q}_s, \mathbf{q}_e$ and tangents $\mathbf{t}_s, \mathbf{t}_e$, and any desired arc length $S > |\mathbf{q}_e - \mathbf{q}_s|$, through a simple algorithm. This algorithm plays a key role in the construction of helical paths with specified axes, pitch angles, and end states by a "lifting" process. The algorithm may be summarized as follows (see [10] for the derivations and complete details).

Using the complex representation with $\mathbf{q}_s = x_s + \mathrm{i}\, y_s$, $\mathbf{q}_e = x_e + \mathrm{i}\, y_e$ and $\mathbf{t}_s = \exp(\mathrm{i}\,\phi_s)$, $\mathbf{t}_e = \exp(\mathrm{i}\,\phi_e)$, and setting $\Delta\mathbf{q} = \mathbf{q}_e - \mathbf{q}_s := |\Delta\mathbf{q}| \exp(\mathrm{i}\,\gamma)$, the prescribed data is first reduced to canonical form by: (i) subtracting $\mathbf{q}_s$ from $\mathbf{q}_s$ and $\mathbf{q}_e$; (ii) dividing $\mathbf{q}_e$ by $\Delta\mathbf{q}$; (iii) multiplying $\mathbf{t}_s$ and $\mathbf{t}_e$ by $\exp(-\mathrm{i}\,\gamma)$; and (iv) dividing S by $|\Delta\mathbf{q}|$. This amounts to a translation/rotation/scaling, that maps $\mathbf{q}_s$ and $\mathbf{q}_e$ to the points 0 and 1 on the real axis. Once the canonical form solution has been computed, it can be restored to the original coordinates by multiplying $\mathbf{w}_0, \mathbf{w}_1, \mathbf{w}_2$ with $\sqrt{|\Delta\mathbf{q}|}\exp(\mathrm{i}\,\frac{1}{2}\gamma)$ before substituting in (5) with the choice $\mathbf{p}_0 = \mathbf{q}_s$. For brevity, only the generic case $\phi_e \neq \pm\,\phi_s$ is considered here (see [10] for treatment of the special cases $\phi_e = \pm\,\phi_s$).

For canonical form data, the coefficients in (2) are written in the form

$$\mathbf{w}_0 \;=\; w\exp(\mathrm{i}\tfrac{1}{2}\phi_s)\,, \quad \mathbf{w}_1 \;=\; u + \mathrm{i}\,v\,, \quad \mathbf{w}_2 \;=\; w\exp(\mathrm{i}\tfrac{1}{2}\phi_e)\,. \tag{9}$$

Assigning $\mathbf{w}_0$ and $\mathbf{w}_2$ to be of equal magnitude ensures that $|\mathbf{p}'(0)| = |\mathbf{p}'(1)|$, so symmetric data yields symmetric interpolants. The real values u, v, w in (9) will be determined as follows. Writing $(\lambda_s, \mu_s) := (\cos\frac{1}{2}\phi_s, \sin\frac{1}{2}\phi_s)$ and $(\lambda_e, \mu_e) := (\cos\frac{1}{2}\phi_e, \sin\frac{1}{2}\phi_e)$, set

$$w \;=\; \sqrt{z}\,, \tag{10}$$

where z is the *smaller* root of the quadratic equation[2]

$$a_2 z^2 + a_1 z + a_0 \;=\; 0 \tag{11}$$

with the coefficients

$$\begin{aligned}
a_2 \;&=\; 2(\lambda_s\mu_e - \lambda_e\mu_s)^2\,,\\
a_1 \;&=\; 3\,[\,2(\lambda_s\lambda_e + \mu_s\mu_e - 3)S + 3(\lambda_s^2 - \mu_s^2 + \lambda_e^2 - \mu_e^2) - 2(\lambda_s\lambda_e - \mu_s\mu_e)\,]\,,\\
a_0 \;&=\; 36(S^2 - 1)\,.
\end{aligned}$$

[2]It is shown in [10] that this equation always has real roots, since the discriminant is always non–negative, and that the roots are both positive.

Then choose $\alpha, \beta = \pm 1$ such that $\alpha\beta$ and $(\lambda_s\mu_e + \lambda_e\mu_s - 3\lambda_s\mu_s - 3\lambda_e\mu_e)z$ are of the same sign. For each of the two α, β pairs thus identified, set

$$u = \frac{-3(\lambda_s + \lambda_e)w + \alpha\sqrt{P(z)}}{4}, \quad v = \frac{-3(\mu_s + \mu_e)w + \beta\sqrt{Q(z)}}{4}, \qquad (12)$$

where

$$P(z) = 60(S+1) - (15\lambda_s^2 + 15\lambda_e^2 - 10\lambda_s\lambda_e)z\,, \qquad (13)$$

$$Q(z) = 60(S-1) - (15\mu_s^2 + 15\mu_e^2 - 10\mu_s\mu_e)z\,. \qquad (14)$$

It may be shown [10] that expressions (13) and (14) are both non–negative at the smaller root of (11). When u, v, w are determined from (10) and (12), the complex coefficients (9) are known, and are multiplied by $\sqrt{|\Delta\mathbf{q}|}\exp(\mathrm{i}\,\frac{1}{2}\gamma)$. The control points $\mathbf{p}_0, \ldots, \mathbf{p}_5$ are then obtained from (5) with $\mathbf{p}_0 = \mathbf{q}_s$.

In general, the procedure provides two formal solutions (corresponding to the two feasible sign pairs α, β) to the problem of matching the specified data, of which one has an attractive shape, while the other exhibits an undesirable looping behavior — the latter can be discarded on the basis of a higher value for the elastic bending energy [8] or absolute rotation index [18].

4 Constant climb rate paths for UAVs

The theory for helical polynomial curves, based on the quaternion and Hopf map representations, accommodates axis vectors with arbitrary orientations [2, 14, 15, 17, 22]. In the UAV path planning problem, however, the climb rate is constrained mainly by the ability of the propulsive power to overcome gravity, so we may focus exclusively on helical paths with vertical axes — i.e., in terms of an orthonormal basis $(\mathbf{i}, \mathbf{j}, \mathbf{k})$ aligned with the (x, y, z) coordinate directions, we need only consider the case[3] $\mathbf{a} = \mathbf{k}$. This allows us to bypass the more cumbersome methodology for spatial PH curves, and achieve exact constructions of climb–rate–limited UAV paths with specified end conditions through simpler, established algorithms for planar PH curves.

In the UAV path planning context, it is convenient to employ the path *climb angle* $\theta = \frac{1}{2}\pi - \psi$ instead of the helix pitch angle, and we assume that $\theta \in (0, \frac{1}{2}\pi)$. The helicity condition (1) then becomes $\mathbf{k}\cdot\mathbf{t}(\xi) \equiv \sin\theta$. We shall consider here only *polynomial* helical curves, and thus exclude the familiar

[3]The generalization to helical axes of arbitrary orientation is treated in Section 5.

circular helix, which for a prescribed climb angle θ may be parameterized as $\mathbf{r}(\phi) = (\rho\cos\phi, \rho\sin\phi, \rho\,\phi\tan\theta)$ — this is a *transcendental curve*, that is not capable of accommodating arbitrary initial/final path states.

Any plane polynomial curve

$$\mathbf{p}(\xi) \;=\; (x(\xi), y(\xi))$$

with parametric speed $\sigma(\xi) = |\mathbf{p}'(\xi)|$ and cumulative arc length function

$$s(\xi) \;=\; \int_0^\xi \sigma(t)\;\mathrm{d}t\,,$$

may be "lifted" [32] to define a helical space curve with climb angle θ through the expression

$$\mathbf{r}(\xi) \;=\; (x(\xi), y(\xi), s(\xi)\tan\theta)\,. \tag{15}$$

When $\mathbf{p}(\xi)$ is a PH curve, $s(\xi)$ is a polynomial, so $\mathbf{r}(\xi)$ is a polynomial curve. Moreover, the magnitude of its derivative

$$\mathbf{r}'(\xi) \;=\; (x'(\xi), y'(\xi), \sigma(\xi)\tan\theta) \tag{16}$$

is the *polynomial* function

$$|\mathbf{r}'(\xi)| \;=\; \sigma(\xi)\sec\theta\,,$$

so $\mathbf{r}(\xi)$ is a spatial PH curve. The coefficients of the parametric speed and arc length polynomials for the helical curve $\mathbf{r}(\xi)$ are simply those of the planar PH curve $\mathbf{p}(\xi)$, scaled by the factor $\sec\theta$. Likewise, the total arc length of $\mathbf{r}(\xi)$ is just $S\sec\theta$. Note also that the unit tangent of $\mathbf{r}(\xi)$ is

$$\frac{\mathbf{r}'(\xi)}{|\mathbf{r}'(\xi)|} \;=\; \left(\frac{x'(\xi)}{\sigma(\xi)}\cos\theta, \frac{y'(\xi)}{\sigma(\xi)}\cos\theta, \sin\theta\right)\,,$$

which clearly satisfies the helicity condition $\mathbf{k}\cdot\mathbf{r}'(\xi) \equiv \sin\theta\,|\mathbf{r}'(\xi)|$.

From (16) we have $\mathbf{r}''(\xi) = (x''(\xi), y''(\xi), \sigma'(\xi)\tan\theta)$, and noting that

$$\sigma'(\xi) \;=\; \frac{x'(\xi)x''(\xi) + y'(\xi)y''(\xi)}{\sigma(\xi)}\,,$$

the curvature of $\mathbf{r}(\xi)$ can be expressed as

$$\frac{|\mathbf{r}'\times\mathbf{r}''|}{|\mathbf{r}'|^3} \;=\; \frac{|x'y'' - x''y'|}{\sigma^3}\,\cos^2\theta\,,$$

which is simply the (magnitude of) curvature for the planar PH curve $\mathbf{p}(\xi)$, multiplied by the factor $\cos^2\theta$. Also, from the fact [32] that for any helix the ratio of curvature to torsion is $\tan\psi$ $(= \cot\theta)$, the torsion of $\mathbf{r}(\xi)$ is given by

$$\frac{(\mathbf{r}' \times \mathbf{r}'') \cdot \mathbf{r}'''}{|\mathbf{r}' \times \mathbf{r}''|^2} \;=\; \frac{|x'y'' - x''y'|}{\sigma^3} \, \sin\theta \cos\theta \,.$$

To construct a polynomial helical path $\mathbf{r}(\xi)$, $\xi \in [\,0,1\,]$ with climb angle θ between the prescribed start and end points and motion directions

$$\begin{aligned} \mathbf{r}_s \;&=\; (x_s, y_s, z_s)\,, \qquad \mathbf{d}_s \;=\; (\cos\theta\cos\phi_s, \cos\theta\sin\phi_s, \sin\theta)\,, \\ \mathbf{r}_e \;&=\; (x_e, y_e, z_e)\,, \qquad \mathbf{d}_e \;=\; (\cos\theta\cos\phi_e, \cos\theta\sin\phi_e, \sin\theta)\,, \end{aligned} \tag{17}$$

we first construct a *planar* PH curve $\mathbf{p}(\xi) = (x(\xi), y(\xi))$, $\xi \in [\,0,1\,]$ with end points (x_s, y_s), (x_e, y_e) and tangents $(\cos\phi_s, \sin\phi_s)$, $(\cos\phi_e, \sin\phi_e)$. Since the z component of (16) must satisfy

$$\int_0^1 \sigma(\xi) \tan\theta \; \mathrm{d}\xi \;=\; S \, \tan\theta \;=\; \Delta z \,,$$

where $\Delta z = z_e - z_s$, we stipulate that $\mathbf{p}(\xi)$ must also have arc length

$$S \;=\; \Delta z \, \cot\theta \,. \tag{18}$$

If $s(\xi)$ is the polynomial arc length function of the planar PH curve $\mathbf{p}(\xi)$, the desired helical path is obtained by the "lifting" (15) of $\mathbf{p}(\xi) = (x(\xi), y(\xi))$ to $\mathbf{r}(\xi) = (x(\xi), y(\xi), z(\xi))$. To achieve the prescribed altitude change Δz with the prescribed constant climb angle θ, the total arc length S of the planar path $\mathbf{p}(\xi)$ must have the precise value specified by (18).

Now S cannot be smaller than $|\mathbf{q}_e - \mathbf{q}_s|$ and by (18) this implies that, for a feasible helical path between $\mathbf{r}_s$ and $\mathbf{r}_e$ with climb angle θ, the inequality

$$\frac{\Delta z}{|\mathbf{q}_e - \mathbf{q}_s|} \;\geq\; \tan\theta$$

must be satisfied — equivalently, the inclination of the displacement vector $\mathbf{r}_e - \mathbf{r}_s$ with the (x, y) plane cannot be smaller than θ (and can be equal only when the given data (17) are consistent with a linear path).

The constructed helical path may be expressed in Bézier form as

$$\mathbf{r}(\xi) \;=\; \sum_{k=0}^{5} \mathbf{r}_k \binom{5}{k} (1-\xi)^{5-k} \xi^k \tag{19}$$

with the control points

$$\mathbf{r}_k \;=\; (x_k, y_k, s_k \tan\theta)\,, \quad k = 0, \ldots, 5\,, \tag{20}$$

where $\mathbf{p}_k = (x_k, y_k)$ are the control points of the planar PH curve $\mathbf{p}(\xi)$, and s_k are the Bernstein coefficients (7) of its arc length $s(\xi)$.

5 Quaternion representation

It is desirable to cast the constructed helical PH quintic (15) in the standard quaternion form [5, 12] of spatial PH curves, to facilitate compatibility with existing methods, and transformations of the coordinates to accommodate an arbitrary orientation of the helix axis. A spatial PH curve may be generated from a quaternion polynomial $\mathcal{A}(\xi) = u(\xi) + v(\xi)\,\mathbf{i} + p(\xi)\,\mathbf{j} + q(\xi)\,\mathbf{k}$ through the expression[4]

$$\mathbf{r}'(\xi) \;=\; \mathcal{A}(\xi)\,\mathbf{k}\,\mathcal{A}^*(\xi)\,, \tag{21}$$

$\mathcal{A}^*(\xi) = u(\xi) - v(\xi)\,\mathbf{i} - p(\xi)\,\mathbf{j} - q(\xi)\,\mathbf{k}$ being the conjugate of $\mathcal{A}(\xi)$. To define a spatial PH quintic, a quadratic quaternion polynomial is employed in (21), specified in Bernstein form as

$$\mathcal{A}(\xi) \;=\; \mathcal{A}_0(1-\xi)^2 + \mathcal{A}_1 2(1-\xi)\xi + \mathcal{A}_2\xi^2\,, \tag{22}$$

and the Bézier control points in the representation (19) are given in terms of its coefficients [9] by

$$\begin{aligned}
\mathbf{r}_1 \;&=\; \mathbf{r}_0 \;+\; \frac{1}{5}\,\mathcal{A}_0\,\mathbf{k}\,\mathcal{A}_0^*\,,\\
\mathbf{r}_2 \;&=\; \mathbf{r}_1 \;+\; \frac{1}{10}(\mathcal{A}_0\,\mathbf{k}\,\mathcal{A}_1^* + \mathcal{A}_1\,\mathbf{k}\,\mathcal{A}_0^*)\,,\\
\mathbf{r}_3 \;&=\; \mathbf{r}_2 \;+\; \frac{1}{30}(\mathcal{A}_0\,\mathbf{k}\,\mathcal{A}_2^* + 4\,\mathcal{A}_1\,\mathbf{k}\,\mathcal{A}_1^* + \mathcal{A}_2\,\mathbf{k}\,\mathcal{A}_0^*)\,,\\
\mathbf{r}_4 \;&=\; \mathbf{r}_3 \;+\; \frac{1}{10}(\mathcal{A}_1\,\mathbf{k}\,\mathcal{A}_2^* + \mathcal{A}_2\,\mathbf{k}\,\mathcal{A}_1^*)\,,\\
\mathbf{r}_5 \;&=\; \mathbf{r}_4 \;+\; \frac{1}{5}\,\mathcal{A}_2\,\mathbf{k}\,\mathcal{A}_2^*\,,
\end{aligned} \tag{23}$$

[4]We depart from prior practice in using the unit vector $\mathbf{k}$, rather than $\mathbf{i}$, in (21). This amounts to using a different coordinate system, more appropriate to the present context.

where $\mathbf{r}_0$ is a free integration constant. A general scheme for determining the quaternion coefficients $\mathcal{A}_0, \mathcal{A}_1, \mathcal{A}_2$ from the known control points $\mathbf{r}_0, \ldots, \mathbf{r}_5$ of a spatial PH quintic is described in [16]. In the case of the helical PH quintic (15), however, an alternative approach is simpler and more enlightening.

Proposition 1 *A quaternion pre–image polynomial $\mathcal{A}(\xi)$ that generates the helical polynomial curve* (15) *with climb angle θ, by lifting the plane PH curve $\mathbf{p}(\xi)$ constructed from* (2) *and* (3)*, may be defined in terms of the components of $\mathbf{w}(\xi) = a(\xi) + \mathrm{i}\, b(\xi)$ as*

$$\mathcal{A}(\xi) \;=\; f a(\xi) - \frac{b(\xi)}{2f}\,\mathbf{i} + \frac{a(\xi)}{2f}\,\mathbf{j} + f\, b(\xi)\,\mathbf{k}\,, \tag{24}$$

where

$$f \;=\; \sqrt{\tfrac{1}{2}(\tan\theta + \sec\theta)}\,. \tag{25}$$

Proof : Expanding (21), the components of $\mathbf{r}'(\xi)$ are

$$\begin{aligned} x'(\xi) \;&=\; 2\,[\,u(\xi)p(\xi) + v(\xi)q(\xi)\,]\,, \\ y'(\xi) \;&=\; 2\,[\,p(\xi)q(\xi) - u(\xi)v(\xi)\,]\,, \\ z'(\xi) \;&=\; u^2(\xi) - v^2(\xi) - p^2(\xi) + q^2(\xi)\,. \end{aligned} \tag{26}$$

Let $\mathbf{p}(\xi) = (x(\xi), y(\xi))$ be generated by polynomials $a(\xi), b(\xi)$ as in (2)–(3). To ensure agreement of equations (2)–(3) and (16) with (26) we must have

$$\begin{aligned} 2(up + vq) \;&=\; a^2 - b^2\,, \\ 2(pq - uv) \;&=\; 2ab\,, \\ u^2 - v^2 - p^2 + q^2 \;&=\; (a^2 + b^2)\tan\theta\,, \end{aligned} \tag{27}$$

where, for brevity, we omit the dependence of u, v, p, q and a, b on ξ.

Treating the first two conditions in (27) as linear equations for v and p, they have the solutions

$$v \;=\; \frac{(a^2 - b^2)q - 2abu}{2(u^2 + q^2)}\,, \quad p \;=\; \frac{(a^2 - b^2)u + 2abq}{2(u^2 + q^2)}\,. \tag{28}$$

Substituting these expressions into the third condition and simplifying then yields the quadratic equation

$$4(u^2 + q^2)^2 - 4\tan\theta(a^2 + b^2)(u^2 + q^2) - (a^2 + b^2)^2 \;=\; 0$$

in $u^2 + q^2$, with the solutions

$$u^2 + q^2 \;=\; \tfrac{1}{2}(\tan\theta \pm \sec\theta)(a^2 + b^2)\,. \tag{29}$$

Now writing $t = \tan\frac{1}{2}\theta$, we have

$$\tan\theta \;=\; \frac{2t}{1-t^2} \quad \text{and} \quad \sec\theta \;=\; \frac{1+t^2}{1-t^2}\,,$$

and therefore

$$\tan\theta - \sec\theta \;=\; -\,\frac{1-t}{1+t}\,,$$

which is clearly negative for $0 < t < 1$, i.e., $\theta \in (0, \frac{1}{2}\pi)$. On the other hand,

$$\tan\theta + \sec\theta \;=\; \frac{1+t}{1-t}$$

is clearly positive for $\theta \in (0, \frac{1}{2}\pi)$. Thus, only the positive sign in (29) yields real solutions for u and q. Equation (29) evidently has infinitely–many real solutions u and q in terms of a and b. To obtain a simple form for $\mathcal{A}(\xi)$, we choose the particular solution for u and q, with the corresponding solution for v and p from (28), specified by

$$u \;=\; f\,a\,, \quad v \;=\; -\,\frac{b}{2f}\,, \quad p \;=\; \frac{a}{2f}\,, \quad q \;=\; f\,b\,, \tag{30}$$

where f is defined by (25). This solution yields the quaternion polynomial (24) — it is easily verified that the solution (30) satisfies equations (27), and yields $u^2 + v^2 + p^2 + q^2 = (a^2 + b^2)\sec\theta = |\mathbf{r}'|$. The entire family of possible solutions for $\mathcal{A}(\xi)$ is identified in Remark 1 below. ∎

Thus, if a_0, a_1, a_2 and b_0, b_1, b_2 are the Bernstein coefficients of $a(\xi)$, $b(\xi)$ the Bernstein coefficients of the quaternion polynomial (22) are

$$\mathcal{A}_r \;=\; f\,a_r - \frac{b_r}{2f}\,\mathbf{i} + \frac{a_r}{2f}\,\mathbf{j} + f\,b_r\,\mathbf{k}\,, \quad r = 0, 1, 2\,. \tag{31}$$

Remark 1 It should be noted that the polynomial $\mathcal{A}(\xi)$ is not unique. For any η, the quaternion polynomial

$$\tilde{\mathcal{A}}(\xi) \;=\; \mathcal{A}(\xi)\mathcal{Q}(\eta) \quad \text{with } \mathcal{Q}(\eta) \;=\; \cos\eta + \sin\eta\,\mathbf{k}$$

generates the same hodograph: since $\mathcal{Q}(\eta)\,\mathbf{k}\,\mathcal{Q}^*(\eta) = \mathbf{k}$ for all η, we have

$$\tilde{\mathcal{A}}(\xi)\,\mathbf{k}\,\tilde{\mathcal{A}}^*(\xi) \equiv \mathcal{A}(\xi)\,\mathbf{k}\,\mathcal{A}^*(\xi)\,.$$

The non–uniqueness of the pre–image polynomial $\mathcal{A}(\xi)$ is a property common to all spatial PH curves [12].

The quaternion representation may be used to construct interpolants with any desired helical axis $\mathbf{a}$. This is accomplished by mapping the given data $\mathbf{r}_s, \mathbf{r}_e$ and $\mathbf{d}_s, \mathbf{d}_e$ by a rotation that makes $\mathbf{a}$ coincide with $\mathbf{k}$. The interpolation problem is solved for this "canonical" data, and the solution is then mapped back to the original coordinate system by applying the inverse rotation.

The vector $\mathbf{a}$ is mapped on to the vector $\mathbf{k}$ by a unit quaternion $\mathcal{U}$ through the expression

$$\mathcal{U}\,\mathbf{a}\,\mathcal{U}^* \;=\; \mathbf{k}\,.$$

One can verify (see Chapter 5 of [9]) that $\mathcal{U}$ is of the form

$$\mathcal{U} \;=\; \frac{\mathbf{a}+\mathbf{k}}{|\mathbf{a}+\mathbf{k}|}\,(\cos\varphi + \sin\varphi\,\mathbf{a})\,,$$

where the first factor is the unit bisector of $\mathbf{a}$ and $\mathbf{k}$, and in the second factor φ is a free parameter (since there are infinitely–many possible rotations of $\mathbf{a}$ onto $\mathbf{k}$). Setting $\beta = \cos^{-1}\mathbf{a}\cdot\mathbf{k}$, the cases $\varphi = \pm\,\pi$ correspond to great–circle rotations — i.e., rotations about axes perpendicular to the plane spanned by $\mathbf{a}$ and $\mathbf{k}$, through angles β or $2\pi - \beta$. Knowing $\mathcal{U}$ for a chosen φ value, the given data $\mathbf{r}_e - \mathbf{r}_s$ and $\mathbf{d}_s, \mathbf{d}_e$ are replaced by the canonical–form data

$$\mathcal{U}(\mathbf{r}_e - \mathbf{r}_s)\mathcal{U}^*\,, \quad \mathcal{U}\mathbf{d}_s\,\mathcal{U}^*\,, \quad \mathcal{U}\mathbf{d}_e\,\mathcal{U}^*$$

appropriate to a vertical axis. Once the canonical–form interpolant and pre–image polynomial $\mathcal{A}(\xi)$ have been constructed, the solution is mapped back to the original coordinate system by replacing $\mathcal{A}(\xi)$ with $\mathcal{U}^*\mathcal{A}(\xi)$ in (21).

Lemma 1 *Any helical polynomial curve* $\mathbf{r}(\xi) = (x(\xi), y(\xi), z(\xi))$ *with a climb angle* θ *amounts to the lifting* (15) *of the planar PH curve* $\mathbf{p}(\xi) = (x(\xi), y(\xi))$ *with arc length function* $s(\xi)$*.*

Proof : Assume, without loss of generality, the use of a coordinate system in which the z–direction is coincident with the helix axis. The helicity condition for $\mathbf{r}(\xi) = (x(\xi), y(\xi), z(\xi))$ is then

$$\frac{z'(\xi)}{\sqrt{x'^2(\xi) + y'^2(\xi) + z'^2(\xi)}} \;\equiv\; \cos\theta\,.$$

Squaring both sides and re–arranging terms then gives

$$x'^2(\xi) + y'^2(\xi) \;\equiv\; z'^2(\xi)\tan^2\theta\,.$$

Hence, $x'^2(\xi) + y'^2(\xi)$ is the perfect square of the polynomial $\pm z'(\xi)\tan\theta$ — i.e., $\mathbf{p}(\xi) = (x(\xi), y(\xi))$ is a planar PH curve. ■

Remark 2 It is evident from Lemma 1 and expression (24) that every helical polynomial curve is essentially dependent upon just two linearly–independent scalar polynomials, rather than the four components of a general quaternion polynomial $\mathcal{A}(\xi) = u(\xi)+v(\xi)\,\mathbf{i}+p(\xi)\,\mathbf{j}+q(\xi)\,\mathbf{k}$. This property is apparent on choosing a coordinate system with one axis coincident with the helix axis. It was shown in [17] that a linear dependence of the coefficients of the quadratic quaternion polynomial (24), expressed in the form

$$\mathcal{A}_1 \;=\; c_0\mathcal{A}_0 + c_2\mathcal{A}_2$$

for real c_0, c_2 values, is a sufficient condition for the spatial PH quintic defined by (21) to be helical. Moreover, writing the coefficients in scalar–vector form as $\mathcal{A}_r = (a_r, \mathbf{a}_r)$ with $\mathbf{a}_r = a_{rx}\mathbf{i} + a_{ry}\mathbf{j} + a_{rz}\mathbf{k}$ for $r = 0, 1, 2$ allows the helix axis $\mathbf{a}$ and climb angle θ to be identified from

$$\mathbf{a} \;=\; \frac{a_0\mathbf{a}_2 - a_2\mathbf{a}_0 + \mathbf{a}_0\times\mathbf{a}_2}{|a_0\mathbf{a}_2 - a_2\mathbf{a}_0 + \mathbf{a}_0\times\mathbf{a}_2|}$$

and

$$\sin\theta \;=\; \frac{a_0a_{2x} - a_2a_{0x} - a_{0y}a_{2z} + a_{0z}a_{2y}}{|a_0\mathbf{a}_2 - a_2\mathbf{a}_0 + \mathbf{a}_0\times\mathbf{a}_2|}\,.$$

These expressions facilitate the reduction of $\mathcal{A}(\xi)$ to a form that is dependent on only two scalar polynomials.

The form (24) may be used to directly generate helical polynomial curves with vertical axes and given climb angle θ, and then impose any desired axis orientation on them by the quaternion rotation scheme described above. For the interpolation of given G^1 end conditions, however, the construction of a planar PH quintic with the arc length (18) is an essential intermediate step.

6 Rotation–minimizing adapted frames

An adapted rotation–minimizing frame (RMF) on a space curve consists of the tangent vector and two normal plane vectors that have no instantaneous rotation about the tangent. The existence of polynomial curves that possess *rational* adapted RMFs has recently attracted much attention [11]. These are necessarily PH curves (since only the PH curves possess rational tangents) and in certain low–degree cases are identified by constraints on the coefficients of the quaternion polynomial $\mathcal{A}(\xi)$. The helical curves discussed herein admit simple closed–form (though non–rational) adapted RMFs. This may be seen as follows. On any PH curve a rational adapted frame — the *Euler–Rodrigues frame* — may be defined [5] through the expressions

$$(\mathbf{e}_1(\xi), \mathbf{e}_2(\xi), \mathbf{e}_3(\xi)) \;=\; \frac{(\mathcal{A}(\xi)\,\mathbf{i}\,\mathcal{A}^*(\xi), \mathcal{A}(\xi)\,\mathbf{j}\,\mathcal{A}^*(\xi), \mathcal{A}(\xi)\,\mathbf{k}\,\mathcal{A}^*(\xi))}{|\mathcal{A}(\xi)|^2}\,.$$

Here $\mathbf{e}_3(\xi)$ is the curve tangent, and $\mathbf{e}_1(\xi)$, $\mathbf{e}_2(\xi)$ span the curve normal plane. The ERF is the preferred point of departure in studying adapted RMFs, since (unlike the Frenet frame) is non–singular at inflection points. Noting that

$$f^2 + \frac{1}{4f^2} \;=\; \sec\theta \qquad \text{and} \qquad f^2 - \frac{1}{4f^2} \;=\; \tan\theta\,,$$

the ERF on the helical polynomial curve specified by (21) and (24) becomes

$$\begin{aligned}
\mathbf{e}_1 \;&=\; \frac{(a^2-b^2)\sin\theta\,\mathbf{i} + 2\,ab\sin\theta\,\mathbf{j} - (a^2+b^2)\cos\theta\,\mathbf{k}}{a^2+b^2}\,,\\
\mathbf{e}_2 \;&=\; \frac{-\,2\,ab\,\mathbf{i} + (a^2-b^2)\,\mathbf{j}}{a^2+b^2}\,,\\
\mathbf{e}_3 \;&=\; \frac{(a^2-b^2)\cos\theta\,\mathbf{i} + 2\,ab\cos\theta\,\mathbf{j} + (a^2+b^2)\sin\theta\,\mathbf{k}}{a^2+b^2}\,,
\end{aligned}$$

with the parametric derivatives

$$\begin{aligned}
\mathbf{e}_1' \;&=\; \frac{2\sin\theta\,(ab'-a'b)\,[\,-2ab\,\mathbf{i} + (a^2-b^2)\,\mathbf{j}\,]}{(a^2+b^2)^2}\,,\\
\mathbf{e}_2' \;&=\; -\,\frac{2\,(ab'-a'b)\,[\,(a^2-b^2)\,\mathbf{i} + 2ab\,\mathbf{j}\,]}{(a^2+b^2)^2}\,,\\
\mathbf{e}_3' \;&=\; \frac{2\cos\theta\,(ab'-a'b)\,[\,-2ab\,\mathbf{i} + (a^2-b^2)\,\mathbf{j}\,]}{(a^2+b^2)^2}\,.
\end{aligned}$$

The ERF angular velocity $\boldsymbol{\omega}$ is defined in terms of the frame derivatives

$$\frac{\mathrm{d}\mathbf{e}_r}{\mathrm{d}s} \;=\; \frac{\mathrm{d}\xi}{\mathrm{d}s}\frac{\mathrm{d}\mathbf{e}_r}{\mathrm{d}\xi} \;=\; \frac{\mathbf{e}_r'}{|\mathbf{r}'|}\,, \quad r = 1,2,3$$

with respect to arc length s along $\mathbf{r}(\xi)$ through the relations

$$\frac{\mathrm{d}\mathbf{e}_r}{\mathrm{d}s} \;=\; \boldsymbol{\omega} \times \mathbf{e}_r\,, \quad r = 1,2,3\,.$$

Noting that $|\mathbf{r}'(\xi)| = \sigma(\xi)\sec\theta$, where $\sigma(\xi) = a^2(\xi) + b^2(\xi)$ is the parametric speed of the plane curve $\mathbf{p}(\xi)$, and writing $\boldsymbol{\omega} = \omega_1\mathbf{e}_1 + \omega_2\mathbf{e}_2 + \omega_3\mathbf{e}_3$, the ERF has angular velocity components

$$(\omega_1, \omega_2, \omega_3) \;=\; \frac{(\mathbf{e}_2' \cdot \mathbf{e}_3, \mathbf{e}_3' \cdot \mathbf{e}_1, \mathbf{e}_1' \cdot \mathbf{e}_2)}{\sigma\sec\theta} \;=\; \frac{2(ab' - a'b)}{(a^2+b^2)^2}(-\cos^2\theta, 0, \sin\theta\cos\theta)\,.$$

Since the plane curve $\mathbf{p}(\xi)$ has curvature $\kappa = 2(ab'-a'b)/(a^2+b^2)^2$, we obtain $\boldsymbol{\omega} = \kappa\cos\theta\,(-\cos\theta\,\mathbf{e}_1 + \sin\theta\,\mathbf{e}_3)$. Thus, the ERF is rotation–minimizing with respect to $\mathbf{e}_2$, but not with respect to the tangent $\mathbf{e}_3$ of $\mathbf{r}(\xi)$.

However an adapted RMF may be obtained by imposing a continuous rotation of $\mathbf{e}_1, \mathbf{e}_2$ in the normal plane. Setting $\mathbf{f}_3 = \mathbf{e}_3$ and introducing new normal–plane vectors $\mathbf{f}_1, \mathbf{f}_2$ defined by

$$\begin{bmatrix} \mathbf{f}_1 \\ \mathbf{f}_2 \end{bmatrix} \;=\; \begin{bmatrix} \cos\Phi & \sin\Phi \\ -\sin\Phi & \cos\Phi \end{bmatrix} \begin{bmatrix} \mathbf{e}_1 \\ \mathbf{e}_2 \end{bmatrix}\,, \tag{32}$$

where $\Phi(\xi)$ is defined (modulo an integration constant) by

$$\Phi(\xi) \;=\; -\,2\,\sin\theta\,\tan^{-1}\frac{b(\xi)}{a(\xi)}\,. \tag{33}$$

This induces an angular velocity component in the $\mathbf{e}_3$ direction, namely

$$\frac{\mathrm{d}\Phi}{\mathrm{d}s} \;=\; \frac{\Phi'}{(a^2+b^2)\sec\theta} \;=\; -\,\frac{2(ab'-a'b)}{(a^2+b^2)^2}\sin\theta\cos\theta\,,$$

that exactly cancels the $\mathbf{e}_3$ component of the ERF angular velocity.

The theory of rational adapted RMFs on general spatial PH curves yields results analogous to (32) and (33), but without the $\sin\theta$ factor in (33). In the absence of this factor, the rotation matrix in (32) is rational in ξ, and hence the RMF $(\mathbf{f}_1, \mathbf{f}_2, \mathbf{f}_3)$ is rational. For the helical curves considered herein, the $\sin\theta$ factor in (33) precludes (in general) a rational dependence of $\mathbf{f}_1, \mathbf{f}_2$ on ξ, but they can nevertheless be efficiently and exactly computed from (32)–(33).

7 Algorithm and computed examples

The methodology for constructing helical polynomial paths with given climb angle and initial/final states is now summarized by an algorithm outline, and some computed examples with vertical axes are presented to illustrate these paths. The solutions may also be transformed to accommodate any desired orientation of the helical axis, as described in Section 5.

Algorithm

input: start/end points $\mathbf{r}_s = (x_s, y_s, z_s)$, $\mathbf{r}_e = (x_e, y_e, z_e)$; motion directions $\mathbf{d}_s = (\cos\theta\cos\phi_s, \cos\theta\sin\phi_s, \sin\theta)$, $\mathbf{d}_e = (\cos\theta\cos\phi_e, \cos\theta\sin\phi_e, \sin\theta)$ with θ = climb angle.

1. set $\Delta z = z_e - z_s$ and $S = \Delta z \cot\theta$;
2. set $\mathbf{q}_s = x_s + \mathrm{i}\, y_s$, $\mathbf{q}_e = x_e + \mathrm{i}\, y_e$ and $\mathbf{t}_s = \exp(\mathrm{i}\,\phi_s)$, $\mathbf{t}_e = \exp(\mathrm{i}\,\phi_e)$;
3. compute the planar PH quintic $\mathbf{p}(\xi)$ that satisfies $\mathbf{p}(0) = \mathbf{q}_s$, $\mathbf{p}(1) = \mathbf{q}_e$, $\mathbf{t}(0) = \mathbf{t}_s$, $\mathbf{t}(1) = \mathbf{t}_e$ with total arc length S, as described in Section 3;
4. compute the control points (5) of $\mathbf{p}(\xi)$, and coefficients of its parametric speed and arc length $\sigma(\xi)$ and $s(\xi)$ from equations (6) and (7);
5. define the "lifted" helical path $\mathbf{r}(\xi)$ in terms of $\mathbf{p}(\xi) = (x(\xi), y(\xi))$ and $s(\xi)$ by equation (15), and obtain its control points from equation (20);
6. compute the coefficients of the quaternion polynomial (22) defined by (25) and (31) from the coefficients a_0, a_1, a_2 and b_0, b_1, b_2 of the real and imaginary parts of the complex pre–image polynomial (2) of $\mathbf{p}(\xi)$;

output: helical polynomial curve $\mathbf{r}(\xi)$ with constant climb angle θ satisfying $\mathbf{r}(0) = \mathbf{r}_s$, $\mathbf{r}(1) = \mathbf{r}_e$ and $\mathbf{r}'(0) = |\mathbf{r}'(0)|\,\mathbf{d}_s$, $\mathbf{r}'(1) = |\mathbf{r}'(1)|\,\mathbf{d}_e$ together with its control points $\mathbf{r}_0, \ldots, \mathbf{r}_5$ and pre–image quaternion polynomial $\mathcal{A}(\xi)$.

Figure 1 illustrates some example helical paths between given end states constructed using this algorithm. The case on the left corresponds to climb angle $\theta = \frac{1}{4}\pi$ with an increase in altitude $\Delta z = 1.12\tan\theta$ between end points $\mathbf{r}_s = (0.25, 0.25, 0.25)$ and $\mathbf{r}_e = (1.25, 0.25, 0.25 + S\tan\theta)$ having associated motion directions defined by (17) with $\phi_s = \frac{1}{4}\pi$ and $\phi_e = \frac{1}{3}\pi$. The planar PH quintic must have arc length $S = \Delta z \cot\theta = 1.12$, and its construction admits

two formal solutions, with the absolute rotation indices $R_{\text{abs}} = 1.454364$ and 5.360182. The solution with the smaller R_{abs} value is chosen, corresponding to the complex coefficients

$$\begin{aligned} \mathbf{w}_0 &= 1.119619 + 0.463761\,\mathrm{i}\,, \\ \mathbf{w}_1 &= 0.918068 - 1.084742\,\mathrm{i}\,, \\ \mathbf{w}_2 &= 1.049507 + 0.605933\,\mathrm{i}\,. \end{aligned}$$

From these values, the control points (20) of the "lifted" helical path may be computed using (5), (6), and (7).

The case on the right has climb angle $\theta = \frac{1}{5}\pi$ with altitude increase $\Delta z = 1.24 \tan\theta$ between $\mathbf{r}_s = (0.35, 0.35, 0.35)$ and $\mathbf{r}_e = (1.35, 0.35, 0.35 + S\tan\theta)$ with motion directions specified by $\phi_s = -\frac{1}{2}\pi$ and $\phi_e = \frac{1}{3}\pi$. In this case, the planar PH quintic must have arc length $S = 1.24$, and the solution with the smaller R_{abs} value is identified by the complex coefficients

$$\begin{aligned} \mathbf{w}_0 &= 0.697811 - 0.697811\,\mathrm{i}\,, \\ \mathbf{w}_1 &= 1.598173 + 0.146914\,\mathrm{i}\,, \\ \mathbf{w}_2 &= 0.854641 + 0.493427\,\mathrm{i}\,. \end{aligned}$$

Knowing the coefficients $\mathbf{w}_0, \mathbf{w}_1, \mathbf{w}_2$ of the complex polynomial (2) allows its real and imaginary parts $a(\xi)$ and $b(\xi)$ to be used to construct the quaternion pre–image polynomial $\mathcal{A}(\xi)$ in (21) from expressions (24) and (25).

Figure 2 illustrates a family of helical paths with increasing climb angles $\theta = 0.18\pi, 0.20\pi, 0.22\pi, 0.24\pi$ between the end points $\mathbf{r}_s = (0.5, 0.5, 0.5)$ and $\mathbf{r}_e = (1.5, 0.5, 1.7)$ with the altitude increase $\Delta z = 1.2$ and motion directions defined by $\phi_s = -\frac{1}{2}\pi$, $\phi_e = \frac{1}{3}\pi$. It is seen that shallower climb angles result in longer overall path lengths, to ensure satisfaction of the desired climb angle θ — the arc lengths of the planar PH quintics corresponding to the chosen θ values, as defined by (18), are $S = 1.8909$, 1.6517, 1.4506, 1.2779.

Also shown in Figure 2 are a family of helical paths with the same climb angle $\theta = 0.20\pi$ between the points $\mathbf{r}_s = (0.5, 0.5, 0.5)$ and $\mathbf{r}_e = (1.5, 0.5, 1.7)$ that have the same final motion direction $\phi_e = \frac{1}{3}\pi$, but different initial motion directions: $\phi_s = -0.88\pi, -0.80\pi, -0.72\pi, -0.64\pi, -0.56\pi, -0.48\pi$.

8 Closure

A method has been proposed for the construction of polynomial curves with prescribed initial and final positions and directions, that describe constant

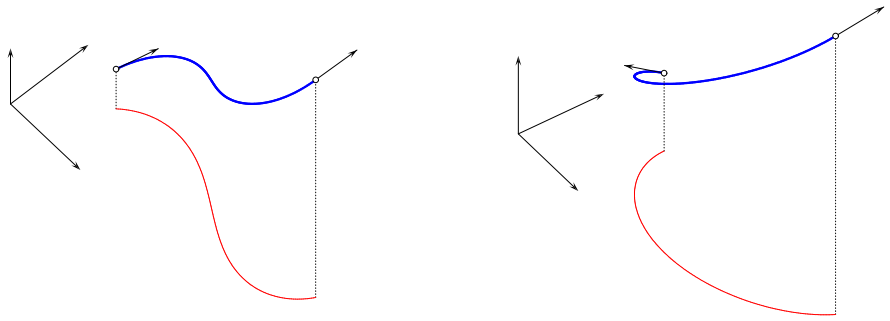

Figure 1: Helical polynomial paths (blue curves) with specified climb angles θ and initial/final positions and directions, generated by the "lifting" of planar PH quintics (red curves) with exactly defined arc lengths and end conditions.

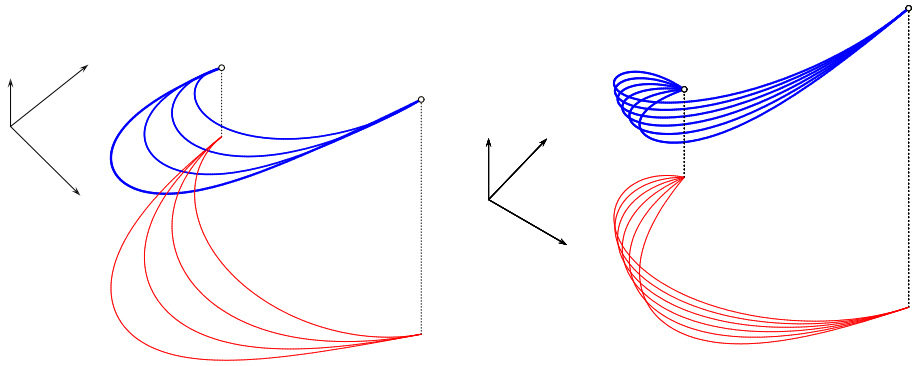

Figure 2: Left: a family of helical paths (blue curves) between specified end points with increasing climb angles, constructed by the "lifting" of planar PH quintics (red curves). Right: helical paths between specified end points with the same climb angles and final directions, but different initial directions.

climb rate paths at a fixed speed for unmanned aerial vehicles. The method relies on the fact that polynomial helical curves are necessarily PH curves, and that the given data may be interpolated by "lifting" a planar PH curve constructed under specific end conditions so as to possess an exact prescribed arc length. The algorithm is simple, efficient, and robust in implementation, and eliminates the need to appeal to numerical approximations.

For compatibility with established spatial PH curve data structures, the quaternion pre–image polynomials of the constructed helical curves are also determined. These allow "canonical" helical interpolants, constructed with a vertical axis, to be transformed so as to accommodate any desired orientation of the axis. The quaternion form also facilitates the identification of closed–form rotation–minimizing adapted frames along the helical paths.

There are several possible directions in which the present algorithm can be extended. For example, instead of prescribing just end points and directions, one may stipulate a sequence of n "waypoints" $\mathbf{r}_1, \ldots, \mathbf{r}_n$ that the path should pass through, with associated directions $\mathbf{d}_1, \ldots, \mathbf{d}_n$. Applying the algorithm to consecutive pairs $\mathbf{r}_k, \mathbf{d}_k$ and $\mathbf{r}_{k+1}, \mathbf{d}_{k+1}$ one obtains a G^1 "helical spline" matching the given data. The method may also be adapted to admit different climb angles and helix axis orientations on individual spline segments, or to achieve greater continuity between spline segments (contingent on the ability to interpolate higher–order geometrical Hermite end–point data using planar PH curves with prescribed arc lengths).

References

[1] A. Askari, M. Mortazavi, H. A. Talebi, and A. Motamedi (2016), A new approach in UAV path planning using Bézier–Dubins continuous curvature path, *J. Aerosp. Eng.* **230**, 1103–1113.

[2] J. V. Beltran and J. Monterde (2007), A characterization of quintic helices, *J. Comput. Appl. Math.* **206**, 116–121.

[3] H. Bruyninckx and D. Reynaerts (1997), Path planning for mobile and hyper–redundant robots using Pythagorean–hodograph curves, *Proceedings, International Conference on Advanced Robotics* (ICAR 97), Monterey, CA, 595–600.

[4] R. Choe, V. Cichella, E. Xargay, N. Hovakimyan, A. C. Trujillo, and I. Kaminer (2013), A trajectory–generation framework for time–critical cooperative missions, *Proceedings, AIAA Infotech Aerospace Conference*, Boston, MA.

[5] H. I. Choi, D. S. Lee, and H. P. Moon (2002), Clifford algebra, spin representation, and rational parameterization of curves and surfaces, *Adv. Comp. Math.* **17**, 5–48.

[6] K. Chu, J. Kim, K. Jo, and M. Sunwoo (2015), Real–time path planning of autonomous vehicles for unstructured road navigation, *Int. J. Automot. Technol.* **16**, 653–668.

[7] R. T. Farouki (1994), The conformal map $z \rightarrow z^2$ of the hodograph plane, *Comput. Aided Geom. Design* **11**, 363–390.

[8] R. T. Farouki (1996), The elastic bending energy of Pythagorean–hodograph curves, *Comput. Aided Geom. Design* **13**, 227–241.

[9] R. T. Farouki (2008), *Pythagorean–Hodograph Curves: Algebra and Geometry Inseparable*, Springer, Berlin.

[10] R. T. Farouki (2016), Construction of G^1 planar Hermite interpolants with prescribed arc lengths, *Comput. Aided Geom. Design* **46**, 64–75.

[11] R. T. Farouki (2016), Rational rotation–minimizing frames — recent advances and open problems, *Applied Math. Comput.***272**, 80–91.

[12] R. T. Farouki, M. al–Kandari, and T. Sakkalis (2002), Structural invariance of spatial Pythagorean hodographs, *Comput. Aided Geom. Design* **19**, 395–407.

[13] R. T. Farouki, C. Giannelli, D. Mugnaini, and A. Sestini (2017), Path planning with Pythagorean–hodograph curves for unmanned or autonomous vehicles, *J. Aerosp. Eng.* to appear.

[14] R. T. Farouki, C. Giannelli, and A. Sestini (2009), Helical polynomial curves and double Pythagorean hodographs I. Quaternion and Hopf map representations, *J. Symb. Comput.* **44**, 161–179.

[15] R. T. Farouki, C. Giannelli, and A. Sestini (2009), Helical polynomial curves and double Pythagorean hodographs II. Enumeration of low–degree curves, *J. Symb. Comput.* **44**, 307–332.

[16] R. T. Farouki, C. Giannelli, and A. Sestini (2015), Identification and "reverse engineering" of Pythagorean–hodograph curves, *Comput. Aided Geom. Design* **34**, 21–36.

[17] R. T. Farouki, C. Y. Han, C. Manni, and A. Sestini (2004), Characterization and construction of helical polynomial space curves, *J. Comput. Appl. Math.* **162**, 365–392.

[18] R. T. Farouki and C. A. Neff (1995), Hermite interpolation by Pythagorean–hodograph quintics, *Math. Comp.* **64**, 1589–1609.

[19] R. T. Farouki and T. Sakkalis (1990), Pythagorean hodographs, *IBM J. Res. Develop.* **34**, 736–752.

[20] D. de A. Fernandes, A. J. Søensen, and D. C. Donha (2013), Path generation for high–performance motion of ROVs based on a reference model, *Model. Ident. Control* **36**, 81–101.

[21] D. G. Macharet, A. A. Neto, and M. F. M. Campos (2009), On the generation of feasible paths for aerial robots in environments with obstacles, *Proceedings, 2009 IEEE/RSJ International Conference on Intelligent Robots and Systems*, Saint Louis, MO, 3380–3385.

[22] J. Monterde (2009), A characterization of helical polynomial curves of any degree, *Adv. Comp. Math.* **30**, 61–78.

[23] A. A. Neto and M. F. M. Campos (2009), A path planning algorithm for UAVs with limited climb angle, *Proceedings, 2009 IEEE/RSJ International Conference on Intelligent Robots and Systems*, Saint Louis, MO, 3894–3899.

[24] A. A. Neto and M. F. M. Campos (2009), On the generation of feasible paths for aerial robots with limited climb angle, *Proceedings, 2009 IEEE International Conference on Robotics and Automation*, Kobe, Japan, 2872–2877.

[25] A. A. Neto, D. G. Macharet, and M. F. M. Campos (2010), Feasible RRT–based path planning using seventh order Bézier curves, *Proceedings, 2010 IEEE/RSJ International Conference on Intelligent Robots and Systems*, Taipei, Taiwan, 1445–1450.

[26] A. A. Neto, D. G. Macharet, and M. F. M. Campos (2010), On the generation of trajectories for multiple UAVs in environments with obstacles, *J. Intell. Robot Syst.* **57**, 123–141.

[27] A. A. Neto, D. G. Macharet, and M. F. M. Campos (2013), Feasible path planning for fixed–wing UAVs using seventh order Bézier curves, *J. Braz. Comput. Soc.* **19**, 193–203.

[28] A. A. Neto, D. G. Macharet, and M. F. M. Campos (2015), 3D path planning with continuous bounded curvature and pitch angle profiles using 7th order curves, *Proceedings, 2015 IEEE/RSJ International Conference on Intelligent Robots and Systems* (IROS), Hamburg, Germany, 4923–4928.

[29] M. Shanmugavel, A. Tsourdos, R. Zbikowski, B. A. White, C. A. Rabbath, and N. Léchevin (2006), A solution to simultaneous arrival of multiple UAVs using Pythagorean hodograph curves, *Proceedings, 2006 American Control Conference*, 2813–2818.

[30] M. Shanmugavel, A. Tsourdos, B. A. White, and R. Zbikowski (2007), Differential geometric path plannings of multiple UAVs, *ASME J. Dyn. Syst. Meas. Control* **129**, 620–632.

[31] M. Shanmugavel, A. Tsourdos, and B. A. White (2010), Collision avoidance and path planning of multiple UAVs using flyable paths in 3D, *Proceedings, 15th International Conference on Methods and Models in Automation and Robotics* (MMAR), Miedzyzdroje, Poland, 218–222.

[32] D. J. Struik (1961), *Lectures on Classical Differential Geometry*, Dover Publications (reprint), New York.

[33] S. Subchan, B. A. White, A. Tsourdos, M. Shanmugavel, and R. Zbikowski (2008), Pythagorean hodograph (PH) planning for tracking airborne contaminant using sensor swarm, *Proceedings, IEEE International Instrumentation and Measurement Control Technology Conference* (I^2MTC 2008).